Solar Energy
and Sustainable Development
Refereed, biannual scientific journal issued by
The Libyan Center for Solar Energy Research and Studies

Geometry-Dependent Thermal Transport in Porous Silicon: A Computational Study of Pore Geometry and Porosity Effects

Othman Soubai[1]*, Younes Abouelhanoune[1], and Mohammed Taibi[1]

[1]LSA, EMAO, ENSAH Al-Hoceima, Abdelmalek Essaadi University, 93000 Tetouan, Morocco.

E-*mail*: [1*]soubai.othman@etu.uae.ac.ma

SPECIAL ISSUE ON.
The 1St International Conference on Sciences and Techniques for Renewable Energy and the Environment.
(STR2E 2025)
May 6-8, 2025 at FST-Al Hoceima-Morocco.

KEYWORDS

Boltzmann transport equation; Thermal transport; Porous Silicon; Thermal management; Semiconductor

ABSTRACT

This study investigates how pore geometry and porosity modulate the thermal conductivity and heat transfer characteristics of porous silicon. Leveraging OpenBTE—an open-source computational tool based on the Boltzmann Transport Equation (BTE)—the research analyzes three distinct pore geometries (circular, rectangular, and hexagonal) with porosity ranging from 5% to 45% in order to quantify their impact on phonon-mediated thermal transport. The results shown a clear dependence of thermal conductivity on pore shape and porosity. Rectangular pores showed the highest thermal conductivity, ranging from 64.4 W/(m·K) at 5% porosity to 26.7 W/(m·K) at 45%. Circular pores yielded intermediate thermal conductivity values, varying from 56.8 W/(m·K) at 5% to 9.5 W/(m·K) at 45%. Hexagonal pores show the lowest thermal conductivity, ranging from 54.6 W/(m·K) to 7.2 W/(m·K). These insights demonstrate the critical role of pore architecture in tailoring heat dissipation pathways, providing actionable guidelines for engineering optimized pore networks. Experimental results advance the understanding of structure-property relationships in porous materials, enabling precise control over thermal performance for applications in thermoelectric, microelectronics, and energy-efficient systems.

*Corresponding author.

DOI: https://doi.org/10.51646/jsesd.v14iSTR2E.1180

النقل الحراري المعتمد على الهندسة في السيليكون المسامي: دراسة حسابية لتأثير هندسة المسام والمسامية

عثمان السبيعي، يونس أبو الحنون، محمد الطيبي

ملخص: تستعرض هذه الدراسة كيفية تأثير هندسة المسام والمسامية على التوصيل الحراري وخصائص نقل الحرارة في السيليكون المسامي، باستخدام أداة "أوبن بي تي إي"، وهي أداة حسابية مفتوحة المصدر تعتمد على معادلة بولتزمان للنقل. قمنا بدراسة ثلاث أشكال هندسية للمسام (دائرية، مستطيلة وسداسية) مع نسب مسامية من 5% إلى 45% لدراسة تأثيرها على النقل الحراري الذي يتم بواسطة الفونونات. أظهرت النتائج علاقة واضحة بين التوصيل الحراري وشكل المسام ونسبة المسامية، إذ سجلت المسام ذات الشكل المستطيل أعلى قيم للتوصيل الحراري التي تتراوح من 64.4 واط/(متر•كلفن) عند نسبة 5% من المسامية إلى 26.7 واط/(متر•كلفن) عند نسبة 45% من المسامية. بينما أعطت للمسام الدائرية قيما متوسطة للتوصيل الحراري، تتراوح من 56.8 واط/(متر•كلفن) عند نسبة 5% من المسامية إلى 9.5 واط/(متر•كلفن) عند نسبة 45% من المسامية. أما بالنسبة للمسام السداسية فقد حققت أدنى قيم للتوصيل الحراري، حيث تراوحت بين 54.6 واط/(متر•كلفن) عند نسبة 5% من المسامية إلى 7.2 واط/(متر•كلفن) عند نسبة 45% من المسامية.

الكلمات المفتاحية: النقل الحراري، السيليكون المسامي، إدارة الحرارة، معادلة بولتزمان للنقل

1. INTRODUCTION

The study of thermal transport properties is essential in many fields of science and engineering and play a critical role in the performance and reliability of microscale and nanoscale devices. With the continued miniaturization of materials and the emergence of novel porous materials such as porous silicon, material systems and devices are entering a nanometer scale, classical macroscopic methods of heat transfer are challenged by size effects and the increased significance of phonon-boundary scattering. which necessitates a thorough understanding of thermal transport at the microscopic level. For micro- or mesoporous media, such as porous silicon, a classical theory based on equivalent macroscopic medium can hardly provide a reliable prediction of the heat transfer coefficient. At the nanoscale, the interplay between intrinsic phonon–phonon interactions and additional scattering mechanisms introduced by porosity requests a refined theoretical framework. This is particularly important for porous silicon, where the high surface area and unique pore geometries, the porosity modifies the material thermal properties, reducing its thermal conductivity by tuning the phonon mean-free path as supported by both experimental and computational studies [1]. Previously reported measurements of the thermal conductivity of Si are primarily carried out as a function of doping density. It is also well established that the thermal conductivity of porous silicon can be significantly reduced in the porous state due to multiple phonon scatterings by the pores [2, 3].

Porous silicon stands out as a multifunctional material not only for its superior heat transfer characteristics but also due to its seamless integration with established manufacturing and device assembly protocols. Its alignment with conventional semiconductor fabrication techniques, combined with its adaptability for use in electronic and photonic systems, positions it as a highly suitable substrate for engineering thermally

optimized [4]. By exclusively studying the distinct pore geometries, we aim to uncover the fundamental mechanisms that govern heat flow, phonon scattering, and thermal conductivity in porous structures [5].

However, while previous measurements have largely emphasized the effects of doping on thermal conductivity, less attention has been paid to how the tortuous pore surfaces and specific geometric configurations of p-Si membranes affects heat transport. This gap in the literature calls for a more detailed computational study that examines pore geometry-dependent heat transport.

A several of studies have shown that increased porosity in porous silicon results in a reduction in thermal conductivity due to enhanced phonon scattering [5, 6]. For example, experimental investigations and computational analyses demonstrated that the thermal behavior of porous silicon can be significantly modified by altering pore size and distribution [5]. Some works have indicated that different pore shapes can alter heat conduction pathways and there by affect the overall thermal performance [7, 8]. These studies suggest that pore geometry plays a critical role in determining thermal performance, but a systematic comparative analysis remains lacking.

The tunable nature of porous silicon—achieved through engineered porosity—has solidified its role in advanced thermal regulation. Customizable pore dimensions, geometries, and spatial arrangements permit fine-grained control overheat dissipation profiles, addressing challenges in sectors such as aerospace, renewable energy infrastructure, and high-density microelectronics [9-12].

Isolating individual pore geometries (e.g., circular, hexagonal, rectangular) provides insights into optimizing composite pore networks for targeted thermal performance. These findings directly inform the design of efficient heat sinks, passive cooling architectures, and precision devices reliant on stable thermal environments [10-12]. Consequently, this systematic investigation of pore driven thermal behavior establishes foundational insights for fabricating next-generation porous silicon membranes, engineered to address escalating demands in thermal management across cutting-edge technologies [13].

By addressing these issues, our study not only confirms the experimentally observed trend of reduced thermal conductivity in porous silicon but also provides new insights into the role of pore geometry. The results have significant implications for the design of thermoelectric materials and microelectronic devices, where controlled thermal management is crucial. Our work contributes to the growing body of research aimed at optimizing the thermal properties of nano porous materials by tuning their structural parameters.

2. METHODOLOGY

2.1. Mathematical Model Theory

In nonmagnetic semiconductor crystals, such as silicon, thermal transport is predominantly facilitated by lattice vibrations, with phonons representing the quantized units of these vibrational modes. In contrast to metals, where electrons play a significant role in heat conduction, the contribution of electrons to thermal conductivity in semiconductors is minimal or negligible at room temperature [14].

The Boltzmann transport equation (BTE) is often used in the modeling of the heat conduction

where the Fourier law breaks down because this law assumes that heat transport is purely diffusive meaning energy carriers (phonon in our case) undergo many collisions as they travel in the materials, this law work well for macroscale system. But when system size is comparable or smaller (our case L=50 nm) than the mean free path (100-300 nm at room temperature in Silicon (Si)). In this case we are in regime where phonons can traverse significant portions of the structure without collisions (ballistic regime), and the presence of pore in our system complicate more the thermal transport. This place our system in the quasi-ballistic transport regime that mean we see a mixture of transport behaviors because our system isn't purely ballistic. Some phonons will still experience collisions with other phonons before reaching a boundary, especially in the regions farther from the pore and in the regions immediately adjacent to the pore, you'll observe largely ballistic transport. Here, phonons travel in straight lines until they encounter either the pore boundary or the system edges.

The Boltzmann Transport Equation (BTE) effectively models both equilibrium and non-equilibrium thermal processes [15]. This framework approximates phonons as discrete particles, neglecting their wave-like characteristics. BTE spans modeling scales from macroscopic continuum regimes to nanoscale systems, as it accounts for both ballistic phonon transport (wave-like propagation without scattering) and diffusive scattering-dominated behavior. This versatility makes BTE particularly suitable for simulating devices or structures that are too small for traditional continuum-based approaches (e.g., Fourier's law) yet too large for fully atomistic simulations like molecular dynamics or quantum mechanical methods [16].

The steady-state, linearized Boltzmann Transport Equation (BTE) under the temperature formulation describes how phonons, the primary heat carriers in non-metallic solids, propagate and scatter within the material. The general form of the BTE for phonon transport can be expressed as:

$$-C_\mu \mathbf{v}_\mu \cdot \nabla \Delta T_\mu(\mathbf{r}) = \sum_\vartheta W_{\mu\vartheta} \Delta T_\vartheta(\mathbf{r}) \quad (1)$$

Where C_μ represents the specific heat capacity of phonon mode μ, $\mathbf{v}_\mu$ is the phonon group velocity, $\nabla \Delta T_\mu(\mathbf{r})$ is the spatial gradient of the temperature deviation for mode μ, and $W_{\mu\vartheta}$ is the scattering matrix element describing the transition rate between phonon modes μ and ϑ.

A commonly used simplification to the phonon Boltzmann transport equation is the relaxation time approximation (RTA), which suppose that phonon repopulation can be neglected. When we use this approximation, the scattering operator is treated as diagonal, meaning that phonon scattering events are supposed to return the system to local equilibrium without any consideration about inter-mode transitions. This approximation is particularly valid for many relevant materials, including silicon, where phonon-phonon scattering dominates the thermal transport [17]. Within the RTA approximation, Equation (1) reduces to:

$$-\mathbf{v}_\mu \cdot \nabla \Delta T_\mu(\mathbf{r}) = \frac{\Delta T_\mu(\mathbf{r}) - \Delta T(\mathbf{r})}{\tau_\mu} \quad (2)$$

Where, τ_μ is the relaxation time for phonon mode μ, is the average time between scattering events. $\Delta T(\mathbf{r})$ is the local temperature deviation from equilibrium, and $\Delta T_\mu(\mathbf{r})$ is the temperature deviation specific to phonon mode μ.

2.1.1. Analytical Study

The solution to Equation (2) under the RTA provides a mathematical approach for calculating the temperature deviation $\Delta T_\mu(\mathbf{r})$ and the resulting heat flux $\mathbf{q}$. This approach enables the calculation of thermal conductivity in porous Silicon by considering the effects of phonon scattering and relaxation times approximation.

The results can be used to analyze the effect of pore geometry and porosity on thermal properties, offering perception for optimizing material design for thermal management applications.

Step 1: Rearrange Equation (2) to isolate $\Delta T_\mu(\mathbf{r})$:

$$\Delta T_\mu(\mathbf{r}) - \Delta T(\mathbf{r}) = -\tau_\mu \mathbf{v}_\mu \cdot \nabla \Delta T_\mu(\mathbf{r}) \tag{3}$$

This can be rewritten as:

$$\Delta T_\mu(\mathbf{r}) = \Delta T(\mathbf{r}) - \tau_\mu \mathbf{v}_\mu \cdot \nabla \Delta T_\mu(\mathbf{r}) \tag{4}$$

For simplicity, assume a linear temperature gradient $\nabla \Delta T(\mathbf{r}) = \mathbf{G}$, where $\mathbf{G}$ is a constant vector representing the applied temperature gradient. This hypothesis is valid for small deviations from equilibrium and is frequently used in thermal transport analysis.

Under this assumption, the temperature deviation $\Delta T(\mathbf{r})$ can be expressed as:

$$\Delta T(\mathbf{r}) = \mathbf{G} \cdot \mathbf{r} \tag{5}$$

Step 2: To solve for $\Delta T_\mu(\mathbf{r})$, we substitute $\Delta T(\mathbf{r}) = \mathbf{G} \cdot \mathbf{r}$ into Equation (4):

$$\Delta T_\mu(\mathbf{r}) = \mathbf{G} \cdot \mathbf{r} - \tau_\mu \mathbf{v}\mu \cdot \nabla \Delta T_\mu(\mathbf{r}) \tag{6}$$

Assuming that $\Delta T_\mu(\mathbf{r})$ has a similar linear form:

$$\Delta T_\mu(\mathbf{r}) = \mathbf{G}_\mu \cdot \mathbf{r} \tag{7}$$

Where $\mathbf{G}_\mu$ is the effective temperature gradient for phonon mode μ. Substituting this into the equation gives:

$$\mathbf{G}_\mu \cdot \mathbf{r} = \mathbf{G} \cdot \mathbf{r} - \tau_\mu \mathbf{v}\mu \cdot \mathbf{G}_\mu \tag{8}$$

Step 3: Since this must hold for all $\mathbf{r}$, we can equate the coefficients of $\mathbf{r}$:

$$\mathbf{G}_\mu = \mathbf{G} - \tau_\mu \left(\mathbf{v}_\mu \cdot \mathbf{G}_\mu\right) \tag{9}$$

This can be written in matrix form as:

$$\left(\mathbf{I} + \tau_\mu \mathbf{v}\mu \otimes \mathbf{v}_\mu\right)\mathbf{G}_\mu = \mathbf{G} \tag{10}$$

Where $\mathbf{I}$ is the identity matrix and $\otimes$ denotes the outer product. Solving for $\mathbf{G}_\mu$:

$$\mathbf{G}_\mu = \left(\mathbf{I} + \tau_\mu \mathbf{v}\mu \otimes \mathbf{v}_\mu\right)^{-1}\mathbf{G} \tag{11}$$

To compute the Heat Flux, the heat flux $\mathbf{q}$ is given by the sum of contributions from all phonon modes:

$$\mathbf{q} = \sum_\mu C_\mu \mathbf{v}\mu \Delta T_\mu(\mathbf{r}) \tag{12}$$

Where C_μ is the specific heat capacity of phonon mode μ. Substituting $\Delta T_\mu(\mathbf{r}) = \mathbf{G}_\mu \cdot \mathbf{r}$:

$$\mathbf{q} = \sum_\mu C_\mu \mathbf{v}_\mu \left(\mathbf{G}_\mu \cdot \mathbf{r}\right) \tag{13}$$

Using the expression for $\mathbf{G}_\mu$:

$$\mathbf{q} = \sum_\mu C_\mu \mathbf{v}_\mu \left[\left(\mathbf{I} + \tau_\mu \mathbf{v}\mu \otimes \mathbf{v}\mu\right)^{-1}\mathbf{G}\right] \cdot \mathbf{r} \tag{14}$$

Step 4: Relate to Thermal Conductivity

The thermal conductivity tensor $\mathbf{K}$ relates the heat flux $\mathbf{q}$ to the temperature gradient

$$\mathbf{q} = -\mathbf{K}\mathbf{G} \tag{15}$$

By comparing this with the expression for $\mathbf{q}$, we can extract the thermal conductivity tensor:

$$\mathbf{K} = -\sum_\mu C_\mu \mathbf{v}\mu \otimes \left(\mathbf{I} + \tau_\mu \mathbf{v}\mu \otimes \mathbf{v}_\mu\right)^{-1} \tag{16}$$

2.2. Numerical Approach

To solve the phonon Boltzmann Transport Equation (BTE). Even after using the relaxation time approximation, is a difficult task due to the high dimensionality of this partial differential equation (PDE), a numerical approach is necessary due to the complexity of the governing equations and the need to account for multiple phonon modes, scattering mechanisms, and geometric effects. Numerous computational approaches have been developed to address this challenge, broadly categorized into stochastic techniques (e.g., Monte Carlo simulations) and deterministic discretization strategies (e.g., finite-volume or spectral methods) [18, 19]. However, conventional Monte Carlo methods exhibit limitations due to statistical uncertainties and reduced computational efficiency at low Knudsen numbers (Kn), where strict constraints on time-step resolution and spatial meshing hinder performance [20, 21]. On the deterministic side, methods such as the discrete ordinate method (DOM) approximate angular space by dividing it into discrete solid angles to resolve non-equilibrium phonon distributions. Despite their utility, DOM-based approaches and similar frameworks often suffer from slow convergence rates in diffusive transport regimes and demand significant memory allocation for high-resolution simulations [22]. By

introducing OpenBTE, a first-principles multidimensional phonon Boltzmann transport equation (BTE). Solver can handle with space-dependent heat transport deterministically. And calculate the temperature and heat flux, and the mode-resolve effective thermal conductivity. OpenBTE employs the anisotropic Mean Free Path Boltzmann Transport Equation (aMFP-BTE) [21] a method to optimize computational efficiency. By interpolating phonon pseudo-temperatures onto vectorial mean free path (MFP) space, this approach reduces the computational cost while preserving accuracy and the upwind finite-volume discretization of Eq. 2.

The discretization of aMFP-BTE model in real and momentum space yields the following iterative linear system [4]

$$A_{ml}\Delta T_{ml}^{(n)} = \sum_{m'l'} S_{ml}^{m'l'}\Delta T_{m'l'}^{(n-1)} + P_{ml} \tag{17}$$

Where A_{ml} is the stiffness matrix for a given MFP and direction, $S_{ml}^{m'l'}$ is associated to the lattice temperature and adiabatic boundary conditions, and P_{ml} represents the perturbation due to the applied temperature gradient. Once Eq 4 converges, the effective thermal conductivity is computed as

$$k_{eff} = \frac{k_{bal}}{2} + \sum_{ml} K_{ml}^{T} \cdot \Delta T_{ml} \tag{18}$$

Where k_{bal} is the ballistic thermal conductivity, K_{ml} is associated to thermal flux. The first guess to Eq. 4 is given by the standard heat conduction equation. OpenBTE solves this system iteratively, leveraging LU factorization for the stiffness matrix and parallel computation via MPI4Py for efficient runtime.

3. THERMAL TRANSPORT IN POROUS SILICON

Thermal transport in porous silicon is a complex phenomenon that need computational tools to model the interplay between phonon scattering mechanisms and material geometry. The numerical simulations utilized the OpenBTE framework, a Boltzmann transport equation solver, which incorporated first-principles-derived material properties for porous silicon. Prior studies [24-26] have documented the development and experimental validation of the OpenBTE framework. The numerical framework accounted for four distinct phonon scattering mechanisms: (1) three-phonon interactions, (2) mass impurity scattering (elastic), (3) grain boundary scattering, and (4) pore-induced scattering. Physical pore obstacles were explicitly represented in the simulation domain, while the first three mechanisms were addressed through the single relaxation time approximation. Matthiessen's rule was applied to combine scattering rates from these three processes. The 2nd and 3rd order interatomic force constants (IFCs) for crystalline silicon were sourced from the AlmaBTE repository, calculated via density functional theory within the virtual crystal approximation. For three-phonon scattering processes, AlmaBTE computed the full scattering matrices from third order IFCs, enabling the solution of the linearized Boltzmann transport equation for phonons [27].

The Figure 1 present the mode resolved phonon properties of silicon at room temperature, heat capacity C_μ , scattering times τ_μ , group velocity v_μ and frequencies ω_μ are required for calculating thermal properties of porous silicon via OpenBTE code because they are the input data for Boltzmann transport equation solver (OpenBTE).

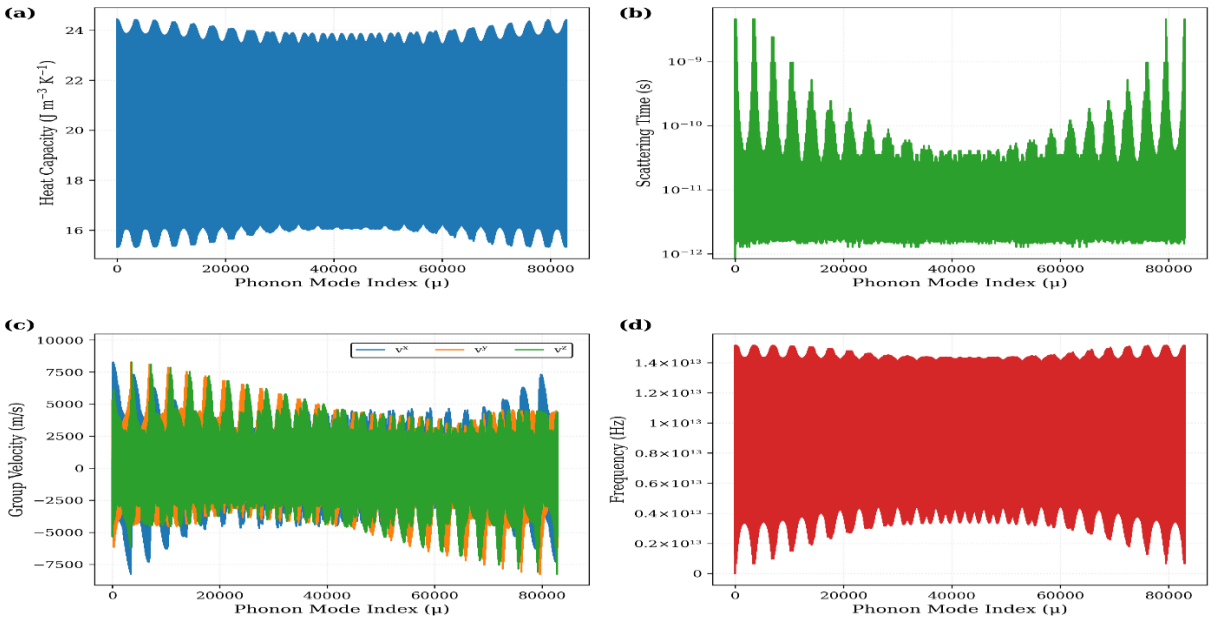

Figure 1: Mode-resolved phonon properties of Si at room temperature using AlmaBTE code [28].
(a) Heat Capacity, (b) Scattering Time, (c) Group Velocity Components, and (d) Frequency Distribution as Functions of Phonon Mode.

The heat capacity presented in figure 2-a is calculated through

$$C_\mu = \frac{k_B}{N_q\, V}\left[\frac{\eta_\mu}{\sinh\left(\eta_\mu\right)}\right]^2, \qquad \eta_\mu = \frac{\hbar\omega_\mu}{2k_B T} \tag{19}$$

And the bulk thermal conductivity tensor is calculated via:

$$k^{\alpha\beta} = \sum_\mu C_\mu \tau_\mu v_\mu^\alpha v_\mu^\beta \tag{20}$$

Where C_μ heat capacity, τ_μ scattering times, v_μ group velocity, ω_μ frequencies and k_B is the Boltzmann constant.

Table 1: Properties for bulk Silicon at room temperature computed using AlmaBTE [28]

Properties	Value
Heat capacity [$Jm^{-3}K^{-1}$]	[24.4476, 24.4476, 24.4476, ..., 15.3429, 15.3429, 15.3338]
Scattering time[s]	[0.00000e+00, 0.00000e+00, 0.00000e+00, ..., 2.60888e-12, 2.52698e-12, 2.34337e-12]
Group velocity[ms^{-1}]	[[0. , 0. , 0.], [0. , 0. , 0.], [0. , 0. , 0.], ..., [141.015, 141.015, 141.015], [263.584, 263.584, 263.584], [120.304, 120.304, 120.304]]
Frequency [s^{-1}]	[0.00000000e+00, 0.00000000e+00, 0.00000000e+00, ..., 1.51217409e+13, 1.51217409e+13, 1.51317995e+13]
Thermal conductivity tensor [$Wm^{-1}K^{-1}$]	[[156.14520455, 0.42324272, 0.42324272], [0.42324272, 156.14520455, 0.42324272], [0.42324272, 0.42324272, 156.14520455]]

3.1. Heat Flux Analysis

Our simulations using a code python to investigate the thermal properties of 2D porous square silicon plate with dimensions of L=50 nm, using tree different pore geometries to see how pore geometry affect heat flux and thermal conductivity.

We use periodic boundary conditions along both axes (x, y), with a temperature difference of 1K applied along the x-direction to drive the thermal transport and because we interest on thermal conductivity along x. Diffuse boundary conditions were applied along all internal pore surfaces to accurately model phonon boundary scattering effects.

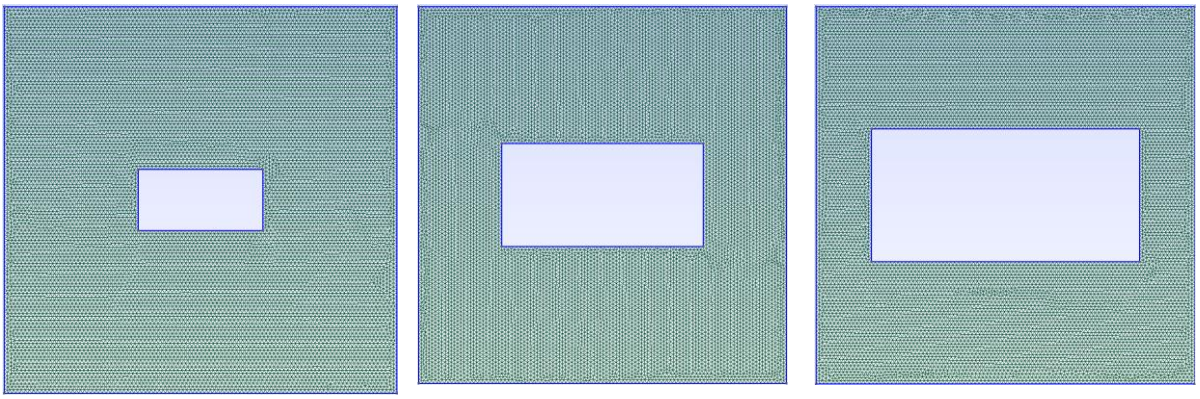

(a) 5% Porosity (b) 15% Porosity (c) 25% Porosity

Figure 2: Mesh Geometry Representations for Rectangular Pore Case using GMSH Code [29].

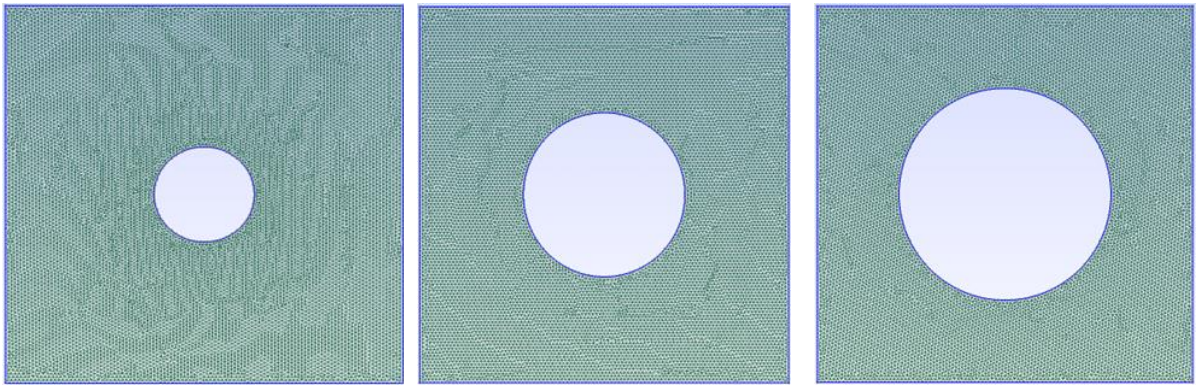

(a) 5% Porosity (b) 15% Porosity (c) 25% Porosity

Figure 3: Mesh geometry representations for circular pore case using GMSH code [29].

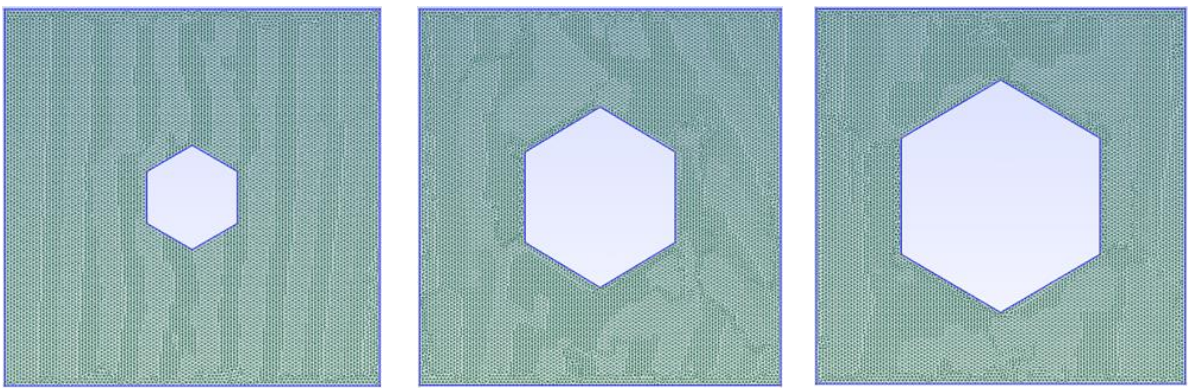

(a) 5% Porosity (b) 15% Porosity (c) 25% Porosity

Figure 4: Mesh geometry representations for hexagonal pore case using GMSH [29].

The system was designed inf Figure 2, 3 and 4 (a, b and c) with a fixed porosity of (5% et 15% 25%) to allow direct comparison between different pore configurations and porosity.

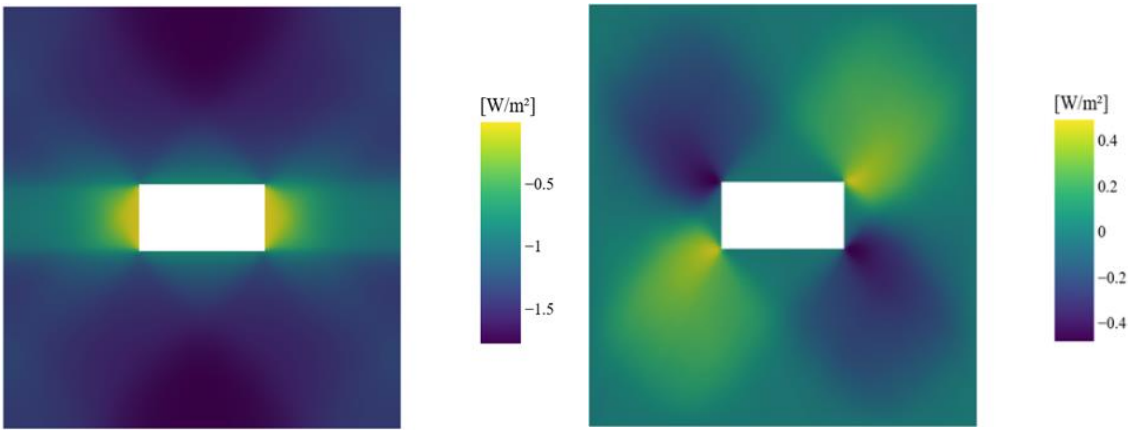

(a) Heat Flux in x-direction (b) Heat Flux in y-direction

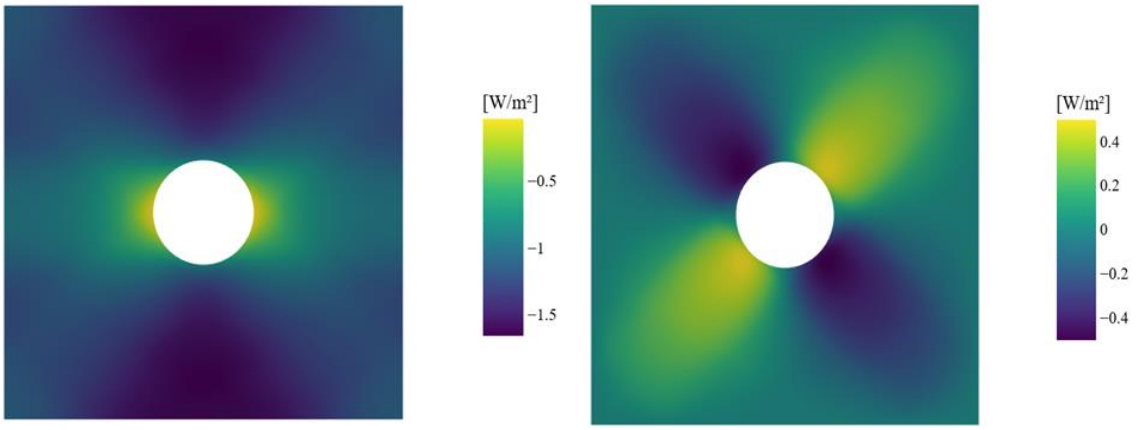

(c) Heat Flux in x-direction (d) Heat Flux in y-direction

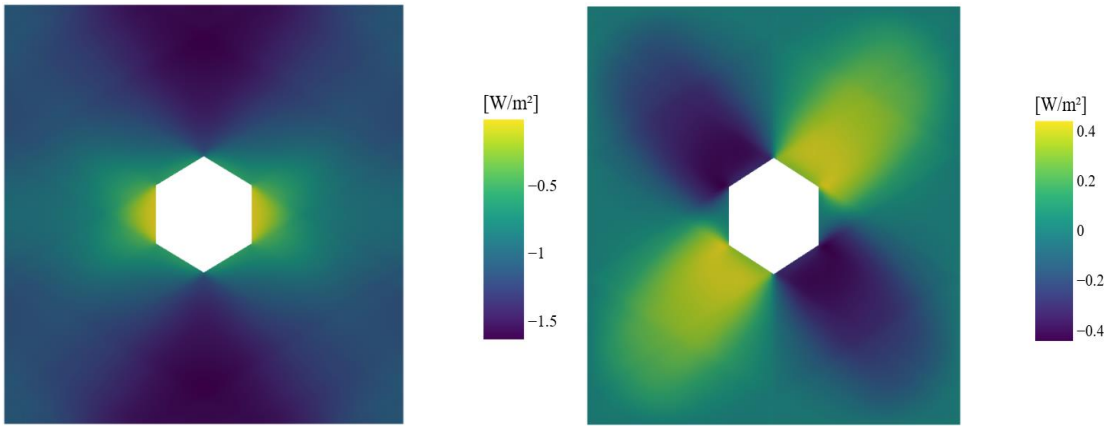

(e) Heat Flux in x-direction (f) Heat Flux in y-direction

Figure 5: Comparative heat flux distributions for different pore geometries at 5% of the porosity.

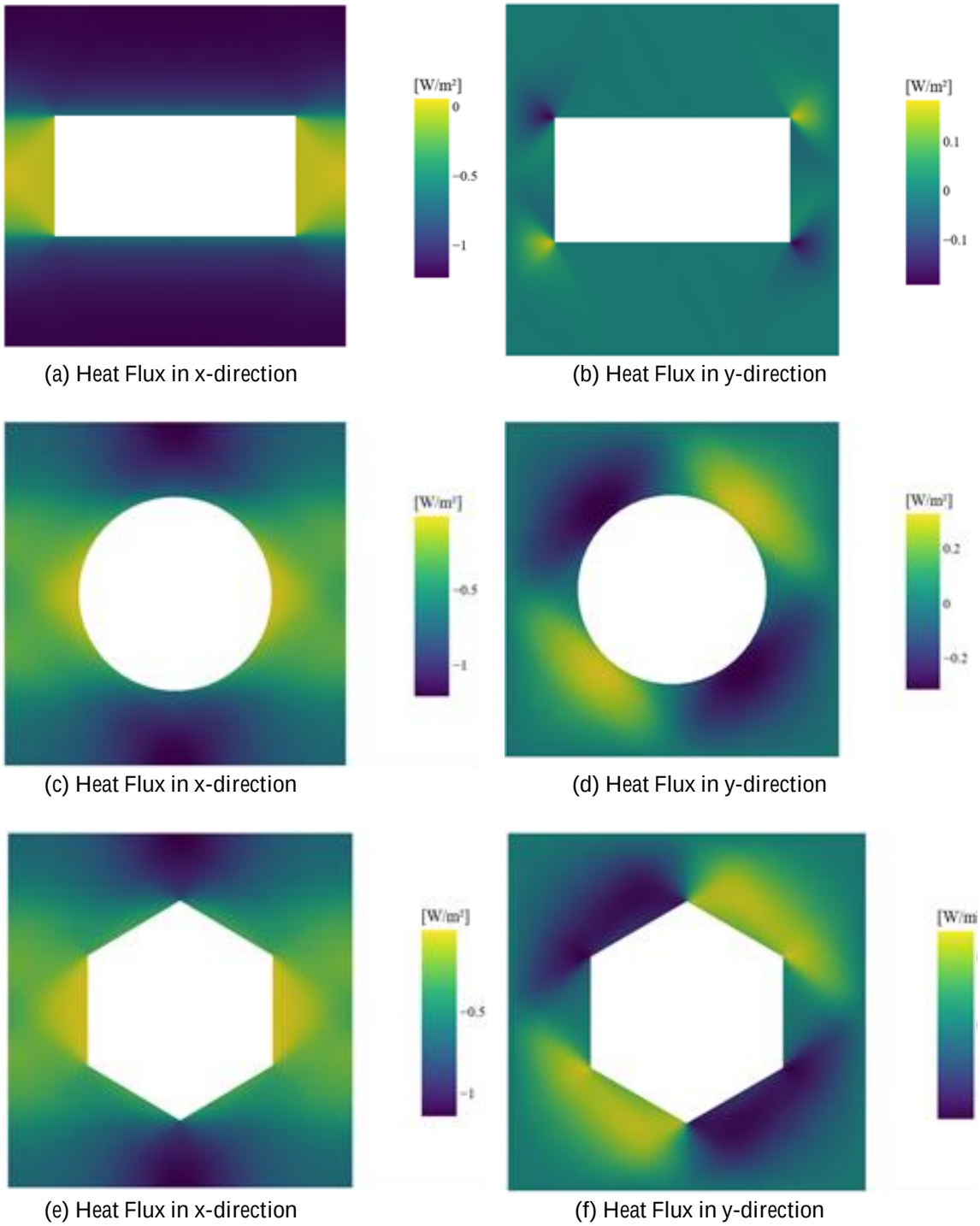

(a) Heat Flux in x-direction (b) Heat Flux in y-direction

(c) Heat Flux in x-direction (d) Heat Flux in y-direction

(e) Heat Flux in x-direction (f) Heat Flux in y-direction

Figure 6: Heat flux in x-direction and in y-direction for porosity 25%

3.1.1. X-Directional Heat Flux Behavior

The x-directional heat flux patterns in subfigures (a, c, e) in Figures (5, 6) reveals how different pore geometries affect thermal transport pathways. The rectangular pore shows concentrated heat flux regions at its vertical edges, with sharp transitions between high and low flux areas but with extended regions of concentrated flux along its longer vertical edges, indicating an enhanced channeling effect due to the increased aspect ratio. The circular pore

demonstrates the most gradual thermal transition profile, with smooth flux distribution around its perimeter, avoiding sharp local concentrations. The hexagonal pore presents an intermediate case, where its angled surfaces create more distributed flux patterns compared to the rectangular and square configurations, yet still maintain some directional preference in heat transport.

3.1.2. Y-Directional Heat Flux Distribution

The analysis of y-directional heat flux patterns in subfigures (b, d, f) in Figures (3-5) reveals a characteristic quadrupolar distribution around all pore shapes, manifested as alternating positive and negative flux regions. This pattern is most symmetrically distributed in the circular pore case, while the rectangular pore shows elongated flux regions corresponding to its extended geometry. The hexagonal geometry displays intermediate patterns and creating more uniform distributions around its six vertices compared to the four corners of the square pore. The rectangular geometry's elongated shape creates an asymmetric quadrupolar pattern, suggesting enhanced vertical heat transport barriers along its longer dimension.

3.2. Thermal Conductivity Analysis

The figure 6 presents a comprehensive comparison of thermal conductivity behavior across three distinct pore geometries (rectangular, circular, and hexagonal), examined over a porosity range of 5% to 45%. The bulk thermal conductivity of silicon, indicated by the dashed line at approximately 154.59 W/(m.K), serves as a reference point for understanding the impact of porosity introduction.

All pore geometries exhibit a consistent trend of decreasing thermal conductivity with increasing porosity, following an approximately linear relationship. This behavior indicates that the volume fraction of void space plays a dominant role in determining thermal transport properties, regardless of pore shape. However, the rate of decrease varies slightly among different geometries, with rectangular pores showing the most gradual decline and hexagonal pores demonstrating the steepest reduction.

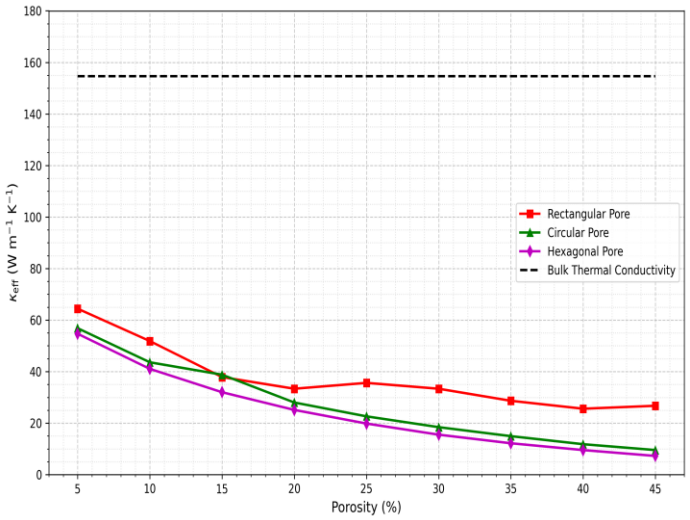

Figure 7: Thermal conductivity of different pore shapes for different porosity

The results demonstrate a clear hierarchy in thermal conductivity values among different pore shapes. The rectangular pore geometry consistently maintains the highest thermal conductivity across all porosity levels, ranging from approximately 64.4 W/(m·K) at 5% porosity to 26.7 W/(m.K) at 45% porosity. This performance preserves the continuous pathways for heat conduction in one primary direction.

The circular pore is the second highest thermal conductivity values, showing a variation between 56.8 W/(m.K) to 9.5 W/(m.K) over the porosity range. This behavior aligns with our heat flux analysis, where circular pores demonstrated uniform heat distribution patterns with minimal local disruptions.

The hexagonal pores show slightly lower thermal conductivity compared to circular pores, with values variations between 54.6 W/(m.K) to 7.2 W/(m.K). This reduction is assigned to the hexagonal geometry that increase phonon scattering.

3.3. Validation and Comparison with Analytical Model

The bulk thermal conductivity of silicon was calculated using the AlmaBTE code, yielding a value of 154.59 W/(m.K). This result shows a very good agreement with experimental data; Chen et al. (2023) reported ~140.2 ± 14.4 W/(m.K) using Raman thermometry [30].

To validate our simulation, we compare the Fourier solver results for circular pore geometry with the analytical model provided by the Eucken–Maxwell model because this analytical model is only applicable for circular pore geometries. The effective thermal conductivity normalized to the bulk value is given by:

$$\frac{k_{eff}}{k_{bulk}} = \frac{1-\emptyset}{1+\emptyset} \tag{21}$$

Where ∅ is the porosity and k_{bulk} is the bulk thermal conductivity.

The following table summarizes the comparison for the circular pore case.

Table 2: Comparison of Fourier Effective Thermal Conductivity

Porosity	Eucken–Maxwell model (W/(m·K))	Fourier solver (W/(m·K))
5%	~139.60	139.8570
15%	~114.18	114.2449
25%	~92.75	92.68315
35%	~74.41	74.14977
45%	~58.69	57.78650

The excellent agreement between the Fourier effective conductivity and the Eucken–Maxwell predictions confirms that the Fourier solver is correctly implemented. But the full solution of the Boltzmann transport equation (BTE) which incorporates non-diffusive effects such as enhanced phonon boundary scattering and ballistic transport that are not captured by Fourier's law. As a result, the effective thermal conductivities obtained from the full BTE

solution are significantly lower.

3.4. Thermal Conductivity Convergence Analysis

3.4.1. Rectangular Pore Case

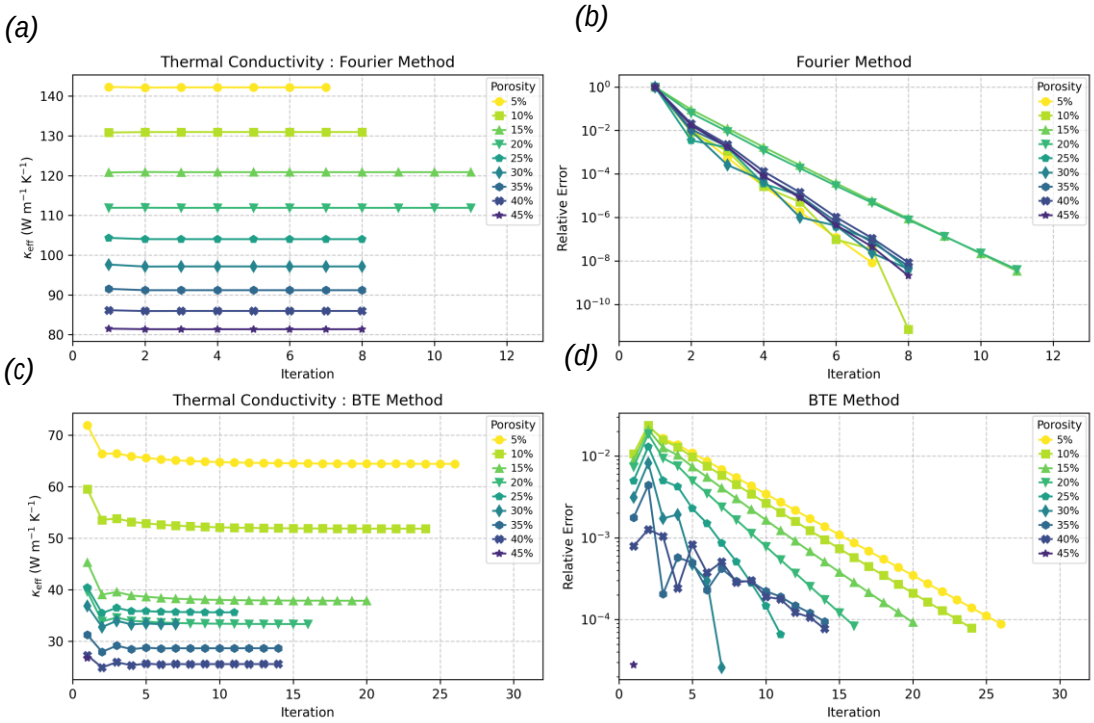

Figure 8: Thermal Conductivity Convergence Analysis for Rectangular Pore at Different Porosities. (a) Convergence of Thermal Conductivity using Fourier, (b) Relative Error in Fourier, (c) Convergence using BTE Method, and (d) Relative Error in BTE Method.

3.4.2. Circular Pore Case

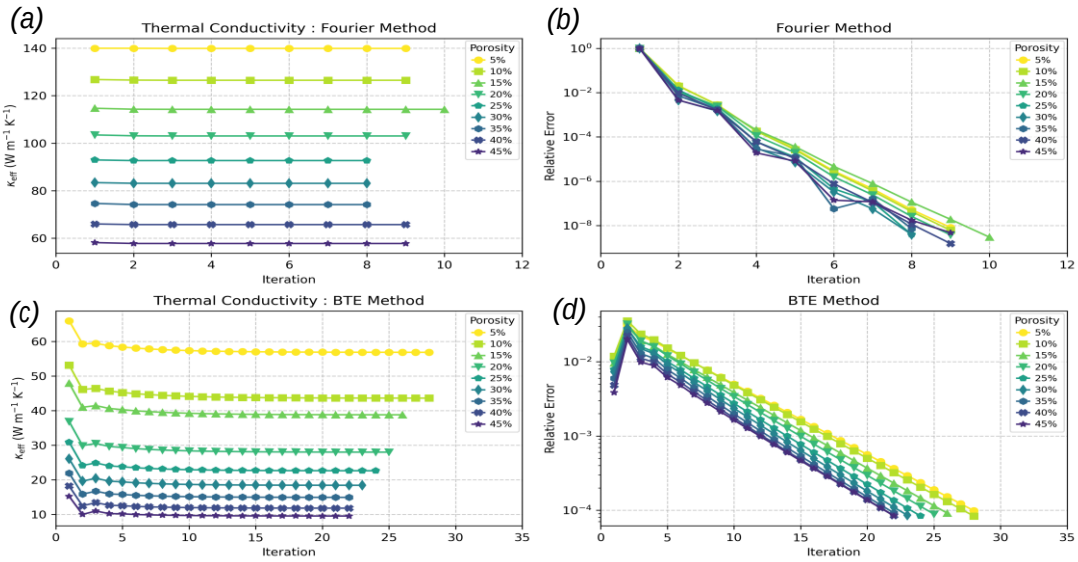

Figure 9: Thermal Conductivity Convergence Analysis for Circular Pore at Different Porosities.

(a) Convergence of Thermal Conductivity using Fourier Method, (b) Relative Error in Fourier Method, (c) Convergence of Thermal Conductivity using BTE Method, and (d) Relative Error in BTE Method.

3.4.3. Hexagonal Pore Case

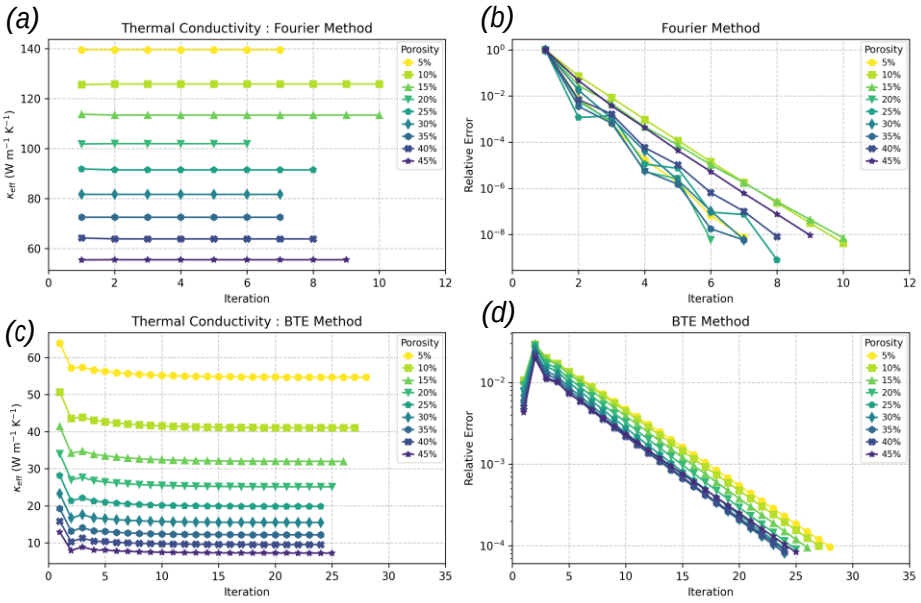

Figure 10: Thermal Conductivity Convergence Analysis for Hexagonal Pore at Different Porosities. (a) Convergence of Thermal Conductivity using Fourier Method, (b) Relative Error in Fourier Method, (c) Convergence of Thermal Conductivity using BTE Method, and (d) Relative Error in BTE

This Results demonstrate that Fourier method converge very quickly take approximately 6 to 10 iterations for all geometry and different porosity making it efficient as an initial guess to solve the problem. The initial error spike in the BTE method indicate the degree of discrepancy between the Fourier method and BTE method and this discrepancy increases as porosity decreases indicate how nanoscale effect become increasingly dominate at lower porosity where the structural dimensions are larger. But the BTE method need more iterations to converge approximately in general take 20 to 25 iterations to converge and, we see that in general low porosity take more iterations to converge but in Fourier we notice that iterations to converge independent to the porosity.

In the BTE method we see also a distinct sensitivity to porosity between 5% to 20% compared to convergence pattern between 25% to 45%. The coupling approach using in OpenBTE Fourier method with BTE show a good computational strategy because the initial Fourier method solutions speed up the convergence of the BTE method by offering a reasonable starting point.

4. CONCLUSIONS

The pore geometry plays a major role in shaping local heat flux distributions in porous Silicon. Circular pores are suitable for applications that requiring a uniform heat distribution, but rectangular pores are suitable for applications that need the directional heat transport pathways. hexagonal pores offer intermediate solutions where hexagonal pores give a more

uniform angular distribution of heat flow.

The study focuses on two aspects of heat transport in porous silicon. First, heat flow patterns are highly sensitive to pore geometry, with circular pores enabling uniform heat distribution and rectangular pores facilitating directional heat flow along their major axes. And second, thermal conductivity with rectangular pores is ideal for scenarios demanding higher thermal conductivity with reduced bulk properties, while hexagonal pores excel in thermal isolation applications where minimal heat conduction is desired. The boundary effects at the Silicon-pore interface vary significantly with geometry. Circular pores promote smooth phonon scattering, while sharp-cornered geometry (hexagonal) induce distinct scattering behaviors that influence thermal resistance.

These results provide a valuable knowledge for optimizing porous silicon structures for specific thermal management applications because the significant reduction in effective thermal conductivity suggests that pore geometry and distribution need to be carefully considered in multi-pore design in porous Silicon, and the complex heat flow patterns observed around the individual pore show that pore-to-pore interactions play an essential role for determining the thermal performance of the porous Silicon. The consistent ordering of thermal conductivity values across all porosity levels suggests that pore geometry and porosity selection can be used to target specific thermal conductivity ranges.

Authors contribution: Othman Soubai: carried out the numerical simulations and contributed to the analysis and validation of the model. Younes Abouelhanoune: Conceptualization of the study, the development of the mathematical model, and the interpretation of the results. Mohammed Taibi: participated in the theoretical framework, literature review, and manuscript drafting. All authors have made an intellectual contribution to the work.

Funding: The authors have not disclosed any funding.

Data Availability Statement: All data are available in the manuscript.

Conflicts of Interest: There are no conflicts to declare.

Acknowledgement: This research was supported through computational resources of HPC-MARWAN provided by the National Center for Scientific and Technical Research (CNRST), Rabat, Morocco. hpc.marwan.ma

REFERENCES

[1] J. Chen and X. Zhang, "Pore-size dependence of the heat conduction in porous silicon and phonon spectral energy density analysis," Physics Letters A, vol. 384, no. 21, p. 126503, 2020. doi: 10.1016/j.physleta.2020.126503

[2] Y. Belaroussi, "High performance porous silicon substrate for the integration of millimeter-wave passive devices," Przegląd Elektrotechniczny, July 2024. doi: 10.15199/48.2024.07.48

[3] E. Amin-Chalhoub et al., "Thermal conductivity measurement of porous silicon by the pulsed-photothermal method," J. Phys. D: Appl. Phys., vol. 44, no. 35, p. 355401, Aug. 2011, doi: 10.1088/0022-3727/44/35/355401.

[4] G. Romano, "Openbte: a solver for ab-initio phonon transport in multidimensional

structures," arXiv preprint arXiv:2106.02764, 2021. https://doi.org/10.48550/arXiv.2106.02764

[5] S. A. Hosseini, S. Khanniche, P. A. Greaney, and G. Romano, "Universal effective medium theory to predict the thermal conductivity in nanostructured materials," International Journal of Heat and Mass Transfer, vol. 183, p. 122040, 2022. https://doi.org/10.3390/thermo4010004

[6] M. Isaiev, N. Kyrychenko, V. Kuryliuk, and D. Lacroix, "Features of phonon scattering by a spherical pore: Molecular dynamics insight," Applied Physics Letters, vol. 124, no. 14, p. 142202, 2024.

[7] Z. Deng, X. Liu, Y. Huang, C. Zhang, and Y. Chen, "Heat Conduction in Porous Media Characterized by Fractal Geometry," Energies, vol. 10, p. 1230, 2017. https://doi.org/10.3390/en10081230

[8] A. Pavlenko, "Heat and Mass Transfer in Porous Materials," Materials, vol. 16, p. 5591, 2023. https://doi.org/10.3390/ma16165591

[9] A. Jain, Y.-J. Yu, and A. J. H. McGaughey, "Phonon transport in periodic silicon nanoporous films with feature sizes greater than 100 nm," Physical Review B, vol. 87, p. 195301, 2013. https://doi.org/10.1103/PhysRevB.87.195301

[10] W. Xing, Y. Xu, C. Song, and T. Deng, "Recent Advances in Thermal Interface Materials for Thermal Management of High-Power Electronics," Nanomaterials, vol. 12, p. 3365, 2022. https://doi.org/10.3390/nano12193365

[11] M. Kashiwagi, Y. Sudo, T. Shiga, and J. Shiomi, "Modeling Heat Conduction in Nanoporous Silicon with Geometry Distributions," Physical Review Applied, 2018. DOI: https://doi.org/10.1103/PhysRevApplied.10.044018

[12] U. Ijaz, M. Siyar, and C. Park, "The power of pores: review on porous thermoelectric materials," RSC Sustainability, vol. 2, no. 4, pp. 852-870, 2024. doi: 10.1039/D3SU00451A

[13] A. S. Fedorov and A. S. Teplinskaia, "Thermal Properties of Porous Silicon Nanomaterials," Materials, vol. 15, no. 23, p. 8678, Dec. 2022. https://doi.org/10.3390/ma15238678

[14] J. M. Ziman, Electrons and Phonons: The Theory of Transport Phenomena in Solids, Oxford University Press, 2001. https://doi.org/10.1093/acprof:oso/9780198507796.001.0001

[15] J.-P. M. Péraud, C. D. Landon, and N. G. Hadjiconstantinou, "Monte carlo methods for solving the boltzmann transport equation," Annual Review of Heat Transfer, vol. 17, pp. 205–265, 2014. doi: 10.1615/AnnualRevHeatTransfer.2014007381

[16] W. Cheng, A. Alkurdi, and P.-O. Chapuis, "Coupling Mesoscopic Boltzmann Transport Equation and Macroscopic Heat Diffusion Equation for Multiscale Phonon Heat Conduction," Nanoscale and Microscale Thermophysical Engineering, vol. 24, no. 3-4, pp. 150-167, 2020. doi: 10.1080/15567265.2020.1836095

[17] Z. Wang, J. E. Alaniz, W. Jang, J. E. Garay, and C. Dames, "Thermal Conductivity of Nanocrystalline Silicon: Importance of Grain Size and Frequency-Dependent Mean Free Paths," Nano Letters, vol. 11, no. 6, pp. 2206-2213, Jun. 2011. doi: 10.1021/nl1045395

[18] S. Mazumder and A. Majumdar, "Monte Carlo study of phonon transport in solid thin films including dispersion and polarization," Journal of Heat Transfer, vol. 123, pp. 749-759, 2001. https://doi.org/10.1115/1.1377018

[19] Q. Hao, G. Chen, and M.-S. Jeng, "Frequency-dependent Monte Carlo simulations of phonon transport in two-dimensional porous silicon with aligned pores," Journal of Applied Physics, vol. 106, p. 114321, 2009. https://doi.org/10.1063/1.3266169

[20] C. Ni and J. Y. Murthy, "Parallel computation of the phonon Boltzmann transport

equation," Numerical Heat Transfer, Part B, vol. 55, pp. 435-456, 2009. DOI:10.1080/10407780902864771

[21] S. V. J. Narumanchi, J. Y. Murthy, and C. H. Amon, "Comparison of Different Phonon Transport Models for Predicting Heat Conduction in Silicon-on-Insulator Transistors," Journal of Heat Transfer, vol. 127, no. 7, pp. 713-723, Jul. 2005. doi: 10.1115/1.1924571

[22] D. Lacroix, K. Joulain, and D. Lemonnier, "Monte Carlo transient phonon transport in silicon and germanium at nanoscales," Physical Review B, vol. 72, p. 064305, 2005. https://doi.org/10.1103/PhysRevB.72.064305

[23] A. Mittal and S. Mazumder, "Monte Carlo Study of Phonon Heat Conduction in Silicon Thin Films Including Contributions of Optical Phonons," Journal of Heat Transfer, vol. 132, p. 052402, 2010. https://doi.org/10.1115/1.4000447

[24] G. Romano, "Efficient calculations of the mode-resolved ab-initio thermal conductivity in nanostructures," arXiv preprint arXiv:2002.08940, 2020. DOI: 10.48550/arXiv.2105.08181

[25] R. A. Duncan et al., "Thermal transport in nanoporous holey silicon membranes investigated with optically induced transient thermal gratings," Journal of Applied Physics, vol. 128, p. 235106, 2020. https://doi.org/10.1063/1.5141804

[26] W. Park et al., "Phonon conduction in silicon nanobeam labyrinths," Scientific Reports, vol. 7, p. 6233, 2017. https://doi.org/10.1038/s41598-017-06479-3

[27] W. Li, J. Carrete, N. A. Katcho, and N. Mingo, "ShengBTE: A solver of the Boltzmann transport equation for phonons," Computer Physics Communications, vol. 185, pp. 1747–1758, 2014. https://doi.org/10.1016/j.cpc.2014.02.015

[28] J. Carrete et al., "almaBTE: A solver of the space–time dependent Boltzmann transport equation for phonons in structured materials," Computer Physics Communications, vol. 220, pp. 351–362, 2017. https://doi.org/10.1016/j.cpc.2017.06.023

[29] C. Geuzaine and J.-F. Remacle, "Gmsh: a three-dimensional finite element mesh generator with built-in pre- and post-processing facilities," International Journal for Numerical Methods in Engineering, vol. 79, no. 11, pp. 1309-1331, 2009. https://doi.org/10.1002/nme.2579

[30] R. An, J. Zhao, J. Yang, S. Zhai, L. Dai, Q. Wang, J. Li, W. Hu, G. Sun, Y. Fan, S. Wu, and G. Niu, "Accurate and wide-range measurement of thermal conductivity of semiconductor materials by laser-excited Raman spectroscopy," Journal of Applied Physics, vol. 134, no. 1, p. 015103, Jul. 2023. doi: 10.1063/5.0152963